Electronic supplementary information for

Heterogeneous water oxidation photocatalysis based on periodic mesoporous organosilica immobilizing a tris(2,2'-bipyridine)ruthenium sensitizer

Minoru Waki,*[a] Soichi Shirai,[a] Ken-ichi Yamanaka,[a] Yoshifumi Maegawa[a] and Shinji Inagaki[a]

[a]Toyota Central R&D Labs., Inc., Nagakute, Aichi 480-1192, Japan.

Experimental section

General. All reagents and solvents were commercially available and used without further purification. XRD patterns were recorded with a Rigaku RINT-TTR diffractometer using Cu Kα radiation (50 kV, 300 mA). Nitrogen adsorption and desorption isotherms were acquired using a Quantachrome Nova3000e sorptometer, and surface areas were calculated from the linear sections of Brunauer-Emmett-Teller (BET) plots (P/P_0 = 0.1–0.2). Pore-size distributions were determined using density functional theory (DFT) (DFT kernel: N_2 at 77 K on silica, cylindrical pores, nonlinear DFT (NLDFT) equilibrium model). Pore volumes were estimated by the t-plot method. FT-IR spectra were obtained with a Thermo Fisher Scientific Nicolet Avatar-360 FT-IR spectrometer using an attenuated total reflection (ATR) attachment. Steady-state absorption spectra and diffuse reflectance spectra were obtained using a spectrophotometer (JASCO, V-670). For solid powder samples, the absorption spectra were evaluated on the basis of the Kubelka-Munk function, $K / S = (1 - r)^2 / 2r$, where K and S are the absorption and scattering coefficients, respectively, and r is the intensity of the diffuse reflectance light. The sample powders were diluted with $BaSO_4$ to avoid saturation of the absorption. Emission spectra were measured using a spectrofluorometer (JASCO, FP-8600). Phosphorescence quantum yield was determined as an average of five measurements with an absolute photoluminescence quantum yield system (Hamamatsu, C9920-01). For the emission and quantum yield measurements of solid powder samples, a dilute suspension of powder was used to avoid reabsorption of the emission. The suspension was prepared by dispersion of the powder samples in H_2O.[S1,S2] The measurements were carried out at room temperature (298 K). Decay curves of the phosphorescence were measured by a time-correlated single photon counting (TCSPC) system (Becker & Hickel, SPC-730 Module) as described elsewhere. The excitation light at 400 nm was obtained from the second harmonic generation output pulse of a mode-locked Ti:sapphire oscillator (Coherent, Vitesse) using 0.5 mm thick β-BaB_2O_4 (BBO) crystal. TEM observations were performed with a JEOL JEM-EX2000 operating at 200 kV.

Preparation for homogeneous ruthenium complexes

$Ru(dmbpy)_2(bpy)(PF_6)_2$. A 50-mL round-bottom-two-necked flask equipped with a magnetic stir bar and a reflux condenser was charged with $[Ru(dmbpy)_2(dmso)Cl]Cl$[S3] (0.23 mmol, 0.14 g) and 2,2'-bipyridine (0.2 mmol, 0.031 g) under Ar atmosphere. Ethanol (15 mL) was added, and the resulting mixture was stirred at 90 °C for 20 h. NH_4PF_6 aqueous solution was added to a reaction mixture at room temperature. The red solid was collected by filtration, washed with H_2O, and dried in vacuum. ^{1}H NMR (400 MHz, DMSO-d_6): δ 8.79 (d, J = 8.24 Hz, 2H), 8.68 (s, 4H), 8.12 (t, J = 7.4 Hz, 2H), 7.71 (d, J = 5.04 Hz, 2H), 7.53-7.48 (m, 6H), 7.33 (t, J = 5.72 Hz, 4H), 3.29 (s, 6 H), 3.27 (s, 6H); ^{13}C

NMR (100 MHz, DMSO-d_6): δ 156.7, 156.2, 156.1, 151.2, 150.4, 150.3, 149.6, 137.6, 128.6, 127.8, 125.1, 124.4, 20.8. ESI-HRMS *m/z* calcd. for $[C_{34}H_{32}F_6N_6PRu]^+$: 771.1383; found: 771.1386.

[Ru(dtbbpy)$_2$(dmso)Cl]Cl. Title compound was prepared according to the procedure in the literature published previously.[S3] A 100-mL round-bottom-two-necked flask equipped with a magnetic stir bar was charged with Ru(dtbbpy)$_2$Cl$_2$ (0.74 mmol, 0.55 g) under Ar atmosphere. DMSO (30 mL) was added, and then the resulting mixture was stirred at 85 °C for 5 h. The solvent was removed in vacuo. The residual red oil was subsequently decanted with diethyl ether (Et_2O). The solidified residue was purified by recrystallization from acetone/Et_2O. ^{1}H NMR (400 MHz, $CDCl_3$) δ 10.06 (d, J = 6.4 Hz, 1H), 9.52 (d, J = 6.0 Hz, 1H), 9.50 (s, 1H), 9.33 (s, 1H), 8.20 (d, J = 1.8 Hz, 1H), 8.14 (d, J =1.8 Hz, 1H), 7.67-7.65 (m, 3H), 7.33 (dd, J = 1.8, 6.0 Hz, 1H), 7.20 (dd, J = 1.8, 5.9 Hz, 1H), 7.09 (d, J = 6.0 Hz, 1H), 3.32 (s, 3H), 2.11 (s, 3H), 1.66 (s, 9H), 1.50 (s, 9H), 1.46 (s, 9H), 1.37 (s, 9H); ^{13}C NMR (100 MHz, $CDCl_3$): 165.1, 163.8, 162.6, 161.7, 158.1, 157.8, 157.3, 156.5, 156.3, 155.7, 155.2, 152.1, 151.7, 148.9, 124.6, 124.1, 124.04, 123.96, 119.7, 119.4, 45.3, 42.2, 36.4, 36.0, 35.4, 35.3, 30.8, 30.6, 30.5, 30.3.

Ru(dtbbpy)$_2$(bpy)(PF$_6$)$_2$. A 50-mL round-bottom-two-necked flask equipped with a magnetic stir bar and a reflux condenser was charged with [Ru(dtbbpy)$_2$(dmso)Cl]Cl (0.23 mmol, 0.18 g) and 2,2'-bipyridine (0.2 mmol, 0.031 g) under Ar atmosphere. Ethanol (15 mL) was added to a reaction mixture, and the resulting mixture was stirred at 90 °C for 20 h. NH_4PF_6 aqueous solution was room temperature. The red solid was collected by filtration, washed with H_2O, and dried in vacuum. ^{1}H NMR (400 MHz, DMSO-*d*6) δ 8.33 (d, J = 8.24 Hz, 2H), 8.20 (s, 4H), 7.97 (t, J = 8.02 Hz, 2H), 7.78 (d, J = 5.52 Hz, 2H), 7.65 (d, J =5.92 Hz, 2H), 7.59 (d, J = 6.44 Hz, 2H), 7.53-7.47 (m, 6H), 1.42 (s, 18H), 1.41 (s, 18H); ^{13}C NMR (100 MHz, DMSO-*d6*): 161.9, 161.9, 156.7, 156.4, 156.3, 151.0, 150.6, 150.5, 137.7, 127.9, 124.9, 124.7, 124.5, 121.92, 121.87, 35.5, 30.1. ESI-HRMS *m/z* calcd. for $[C_{46}H_{56}F_6N_6PRu]^+$: 939.3264; found: 939.3273.

Ru(dmcbpy)$_2$(bpy)(PF$_6$)$_2$. A 50-mL round-bottom-two-necked flask equipped with a magnetic stir bar and a reflux condenser was charged with Ru(dmcbpy)$_2$Cl$_2$[S4] (0.16 mmol, 0.14 g) and 2,2'-bipyridine (0.17 mmol, 0.027 g) under Ar atmosphere. Ethanol (4 mL) and H_2O (4 mL) were added to a reaction mixture, and the resulting mixture was stirred at 90 °C for 20 h. NH_4PF_6 aqueous solution was room temperature. The red solid was collected by filtration, washed with H_2O, and dried in vacuum. ^{1}H NMR (400 MHz, DMSO-*d*6) δ 9.35 (d, J = 6.44 Hz, 4H), 8.85 (d, J = 8.24 Hz, 2H), 8.20 (t, J = 7.56 Hz, 2H), 7.98-7.89 (m, 6H), 7.81 (d, J = 5.04 Hz, 2H), 7.71 (d, J = 5.92 Hz, 2H), 7.50 (t, J = 6.42 Hz, 2H), 3.964 (s, 6 H), 3.958 (s, 6H); ^{13}C NMR (100 MHz, DMSO-*d6*): 165.0, 164.0, 157.2, 157.1, 156.1, 152.9, 152.4, 151.2, 138.9, 138.2, 138.2, 128.2, 126.9, 126.8, 124.8, 124.1, 53.4. ESI-HRMS *m/z* calcd. for $[C_{38}H_{32}F_6N_6PRu]^+$: 947.0977; found: 947.0942.

Computations. The B3LYP functional[S5, S6] was adopted in DFT calculations. The def2-TZVP and def2-SVP basis sets were used for Ru and other elements, respectively.[S7] The solvent effect of water was incorporated using the polarizable continuum model (PCM) throughout the calculations.[S8−10] All calculations were carried out utilizing Gaussian09 program.[S11]

Scheme S1. Molecular structures of model complex, RuBP(X), with X = H, Me, *t*-Bu, or CO_2Me.

References

S1 K.-i. Yamanaka, T. Okada, Y. Goto, T. Tani, S. Inagaki, *Phys. Chem. Chem. Phys.*, 2010, **12**, 11688-11696.

S2 T. Okada, K.-i. Yamanaka, Y. Hirose, Y. Goto, T. Tani, S. Inagaki, *Phys. Chem. Chem. Phys.*, 2011, **13**, 7961-7967.

S3 D. Hesek, Y. Inoue, S. R. L. Everitt, H. Ishida, M. Kunieda and M. G. B. Drew, *J. Chem. Soc., Dalton Trans.*, 1999, 3701-3709.

S4 S. A. MacFarland, F. S. Lee, K. A. W. Y. Cheng, F. L. Cozens and N, P. Schepp, *J. Am. Chem. Soc.*, 2005, **127**, 7065-7070.

S5 A. D. Becke, *J. Chem. Phys.*, 1993, **98**, 5648−5652.

S6 Stephens, F. J. Devlin, C. F. Chabalowski and M. J. Frisch, *J. Phys. Chem.*, 1994, **98**, 11623−11627.

S7 F. Weigend and R. Ahlrichs, *Phys. Chem. Chem. Phys.*, 2005, **7**, 3297-3305.

S8 E. Cancès, B. Mennucci and J. Tomasi, *J. Chem. Phys.*, 1997, **107**, 3032−3041.

S9 J. Tomasi, B. Mennucci and R. Cammi, *Chem. Rev.*, 2005, **105**, 2999−3093.

S10 G. Scalmani and M. J. Frisch, *J. Chem. Phys.*, 2010, **132**, 114110-114111 − 114110-114115.

S11 Gaussian 09, Revision D.01, G. W. T. M. J. Frisch, H. B. Schlegel, G. E. Scuseria, M. A. Robb, J. R. Cheeseman, G. Scalmani, V. Barone, G. A. Petersson, H. Nakatsuji, X. Li, M. Caricato, A.

Marenich, J. Bloino, B. G. Janesko, R. Gomperts, B. Mennucci, H. P. Hratchian, J. V. Ortiz, A. F. Izmaylov, J. L. Sonnenberg, D. Williams-Young, F. Ding, F. Lipparini, F. Egidi, J. Goings, B. Peng, A. Petrone, T. Henderson, D. Ranasinghe, V. G. Zakrzewski, J. Gao, N. Rega, G. Zheng, W. Liang, M. Hada, M. Ehara, K. Toyota, R. Fukuda, J. Hasegawa, M. Ishida, T. Nakajima, Y. Honda, O. Kitao, H. Nakai, T. Vreven, K. Throssell, J. A. Montgomery, Jr., J. E. Peralta, F. Ogliaro, M. Bearpark, J. J. Heyd, E. Brothers, K. N. Kudin, V. N. Staroverov, T. Keith, R. Kobayashi, J. Normand, K. Raghavachari, A. Rendell, J. C. Burant, S. S. Iyengar, J. Tomasi, M. Cossi, J. M. Millam, M. Klene, C. Adamo, R. Cammi, J. W. Ochterski, R. L. Martin, K. Morokuma, O. Farkas, J. B. Foresman, and D. J. Fox, Gaussian, Inc., Wallingford CT, 2016.

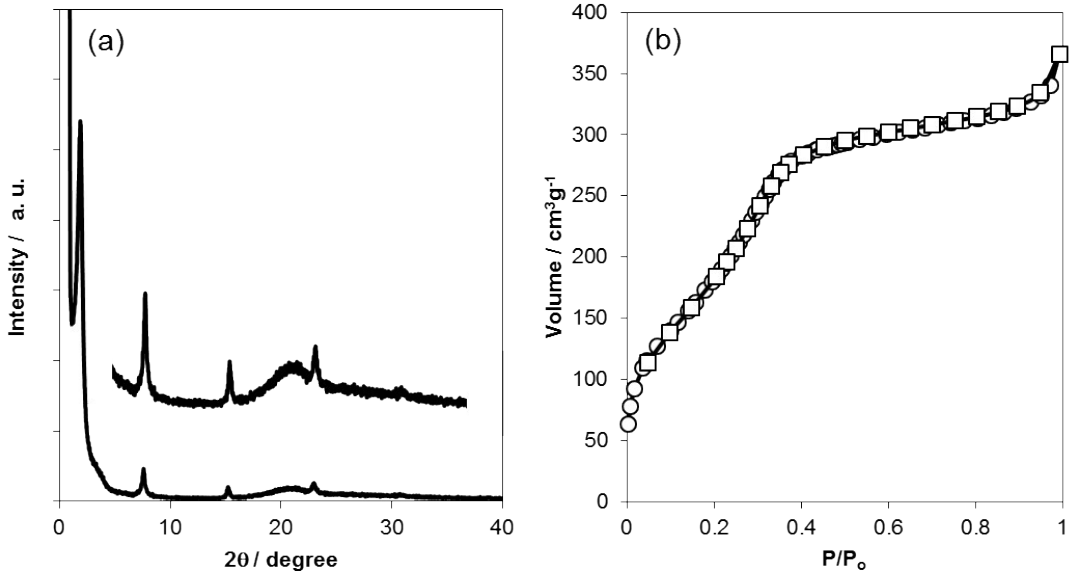

Figure S1. XRD pattern and nitrogen adsorption/desorption isotherms of Ru(H)-BPy-PMO.

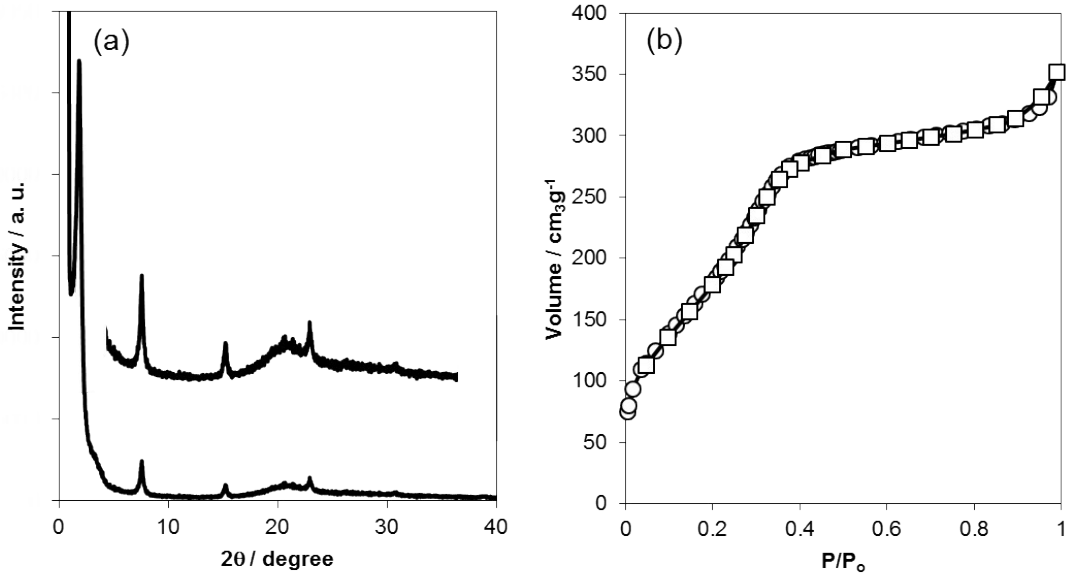

Figure S2. XRD pattern and nitrogen adsorption/desorption isotherms of Ru(Me)-BPy-PMO.

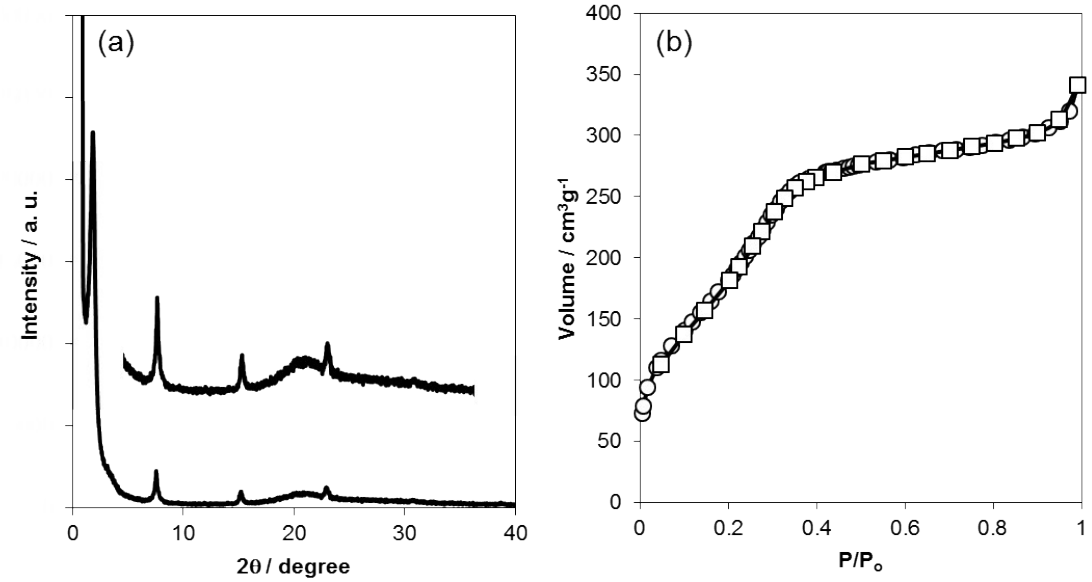

Figure S3. XRD pattern and nitrogen adsorption/desorption isotherms of Ru(*t*-Bu)-BPy-PMO.

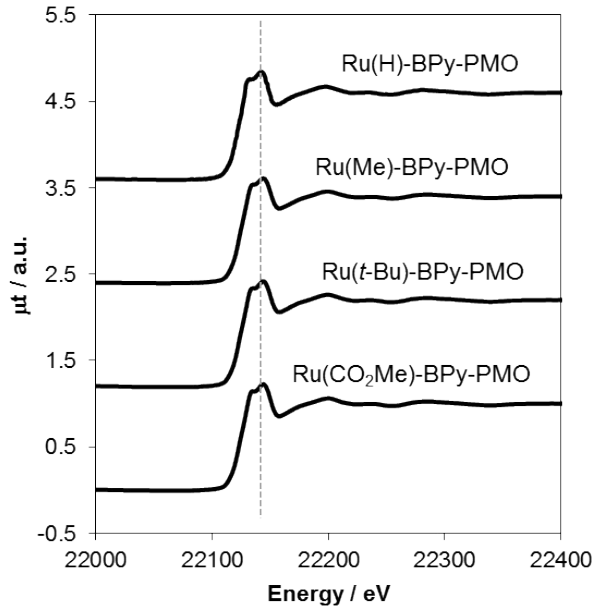

Figure S4 Ru *K*-edge XANES spectra of Ru(X)-BPy-PMOs.

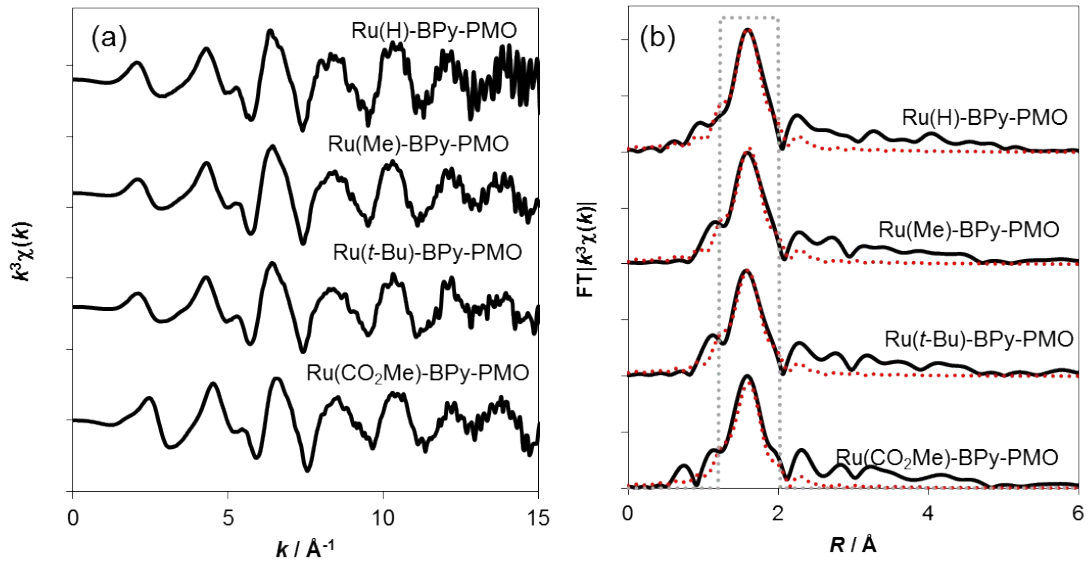

Figure S5 (a) Ru *K*-edge EXAFS oscillations and (b) Fourier transforms with curve fitting of Ru(X)-BPy-PMOs.

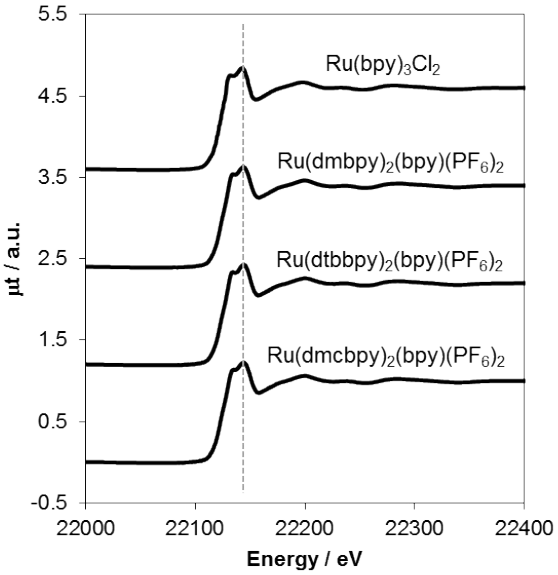

Figure S6 Ru *K*-edge XANES spectra of homogeneous Ru complexes.

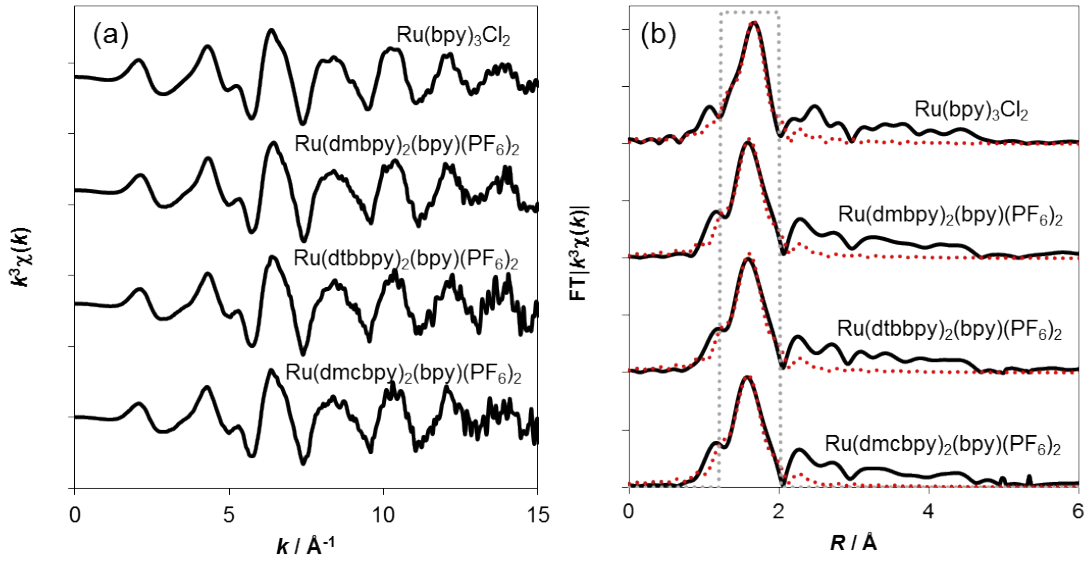

Figure S7 (a) Ru *K*-edge EXAFS oscillations and (b) Fourier transforms with curve fitting of homogeneous Ru complexes.

Table S1

Complex	CN	Distance / Å	ΔE_0 / eV	σ^2 / nm^2
$Ru(bpy)_3Cl_2$	6.13 ± 1.40	2.08 ± 0.009	–0.79 ± 2.73	0.0030 ± 0.0009
$Ru(dmbpy)_2(bpy)(PF_6)_2$	5.94 ± 2.32	2.07 ± 0.014	–2.00 ± 4.47	0.0028 ± 0.0017
$Ru(dtbbpy)_2(bpy)(PF_6)_2$	5.97 ± 1.81	2.07 ± 0.012	–4.38 ± 3.88	0.0023 ± 0.0014
$Ru(dmcbpy)_2(bpy)(PF_6)_2$	5.89 ± 2.86	2.07 ± 0.020	–2.13 ± 5.14	0.0028 ± 0.0020

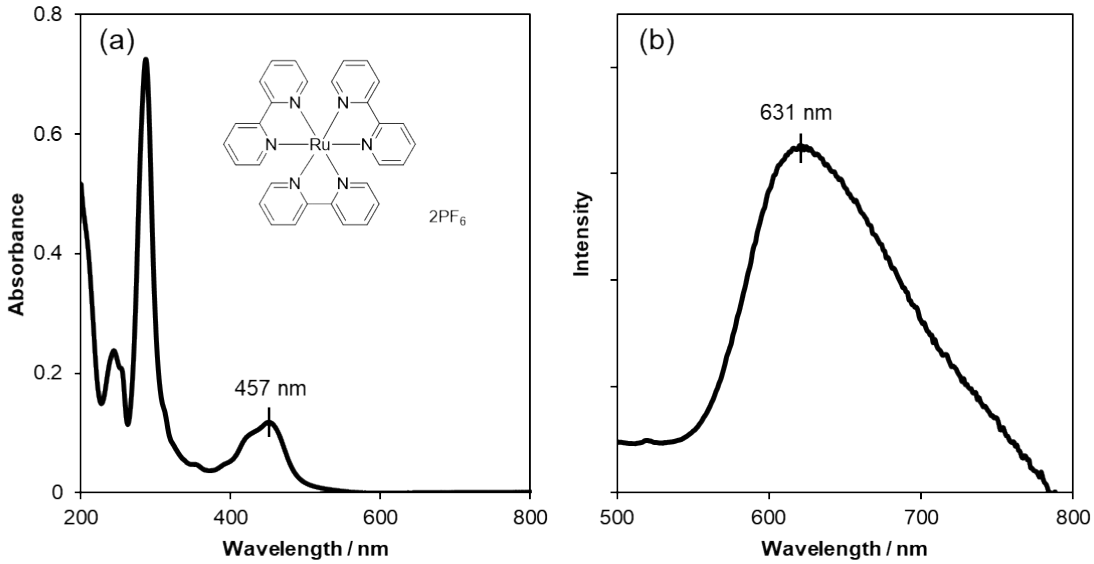

Figure S8 (a) UV/vis absorption and (b) emission spectrum of $Ru(bpy)_3(PF_6)_2$ in CH_3CN (1×10^{-5} M). The excitation wavelength is 450 nm.

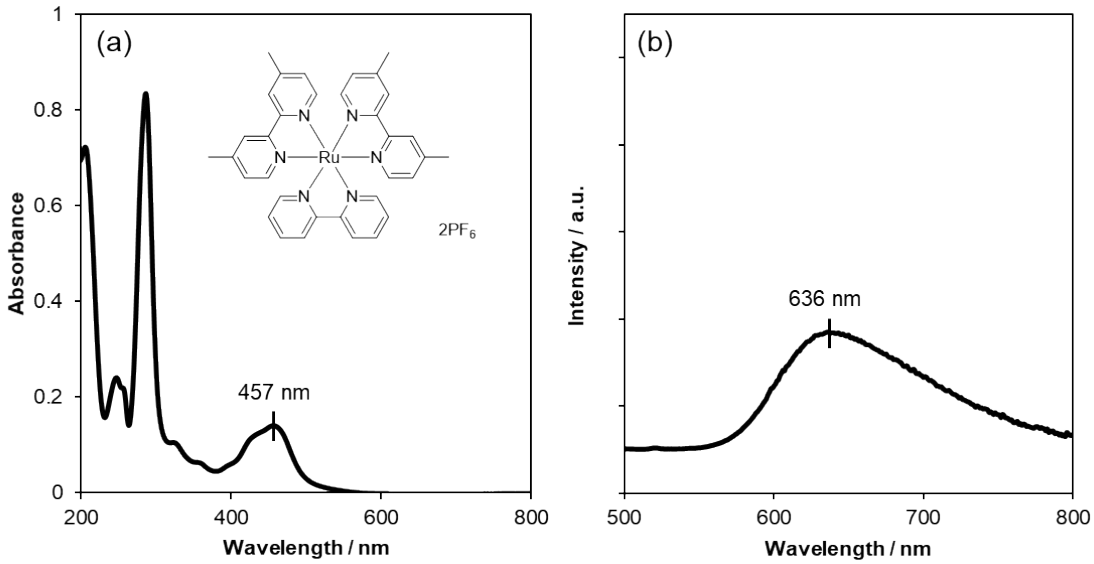

Figure S9 (a) UV/vis absorption and (b) emission spectrum of $[Ru(dmbpy)_2(bpy)](PF_6)_2$ in CH_3CN (1×10^{-5} M). The excitation wavelength is 450 nm.

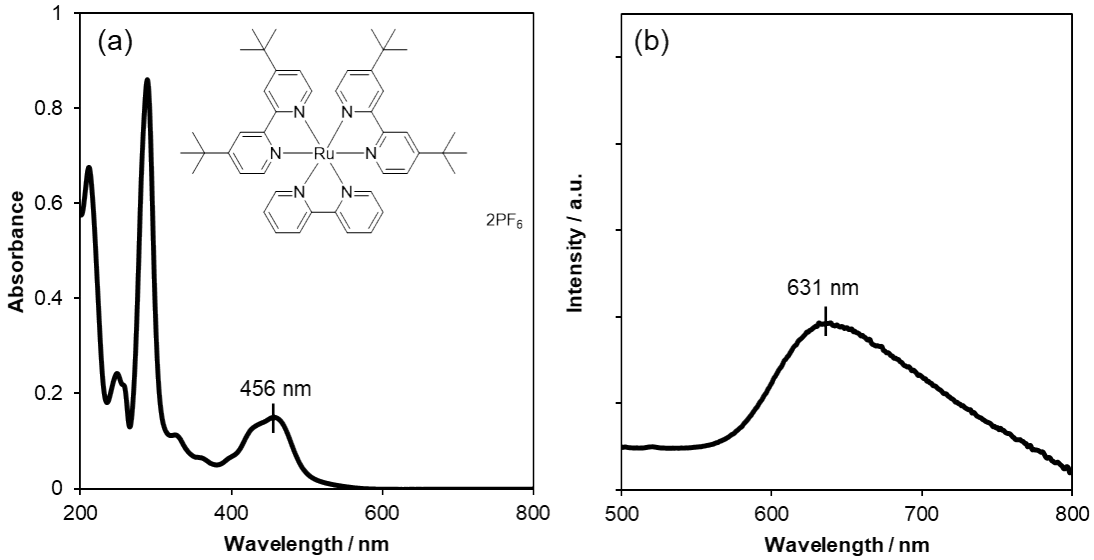

Figure S10 (a) UV/vis absorption and (b) emission spectrum of $[Ru(dtbbpy)_2(bpy)](PF_6)_2$ in CH_3CN (1×10^{-5} M). The excitation wavelength is 450 nm.

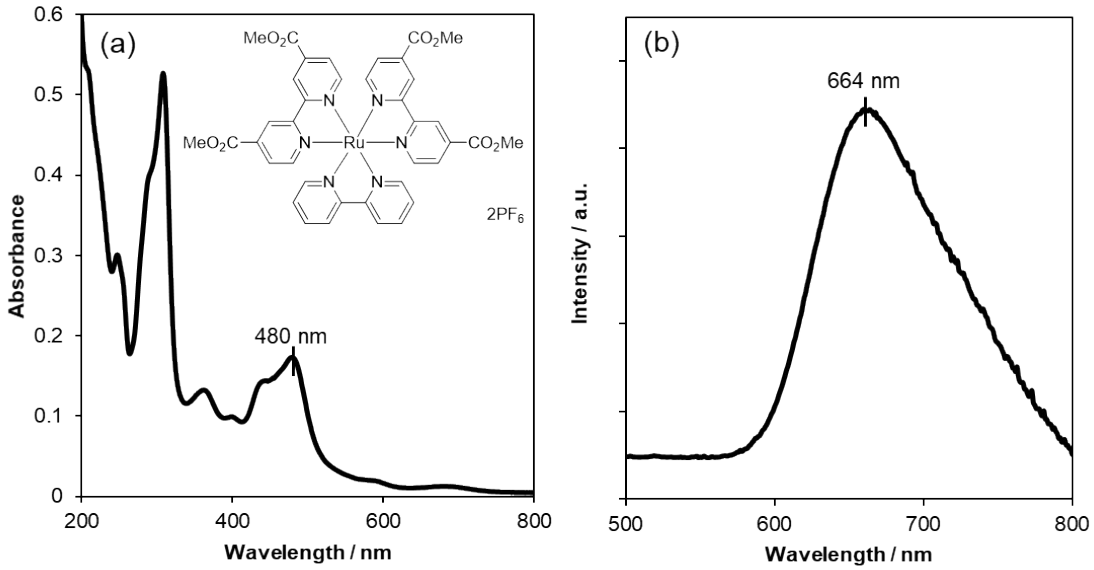

Figure S11 (a) UV/vis absorption and (b) emission spectrum of $[Ru(dmcbpy)_2(bpy)](PF_6)_2$ in CH_3CN (1×10^{-5} M). The excitation wavelength is 450 nm.

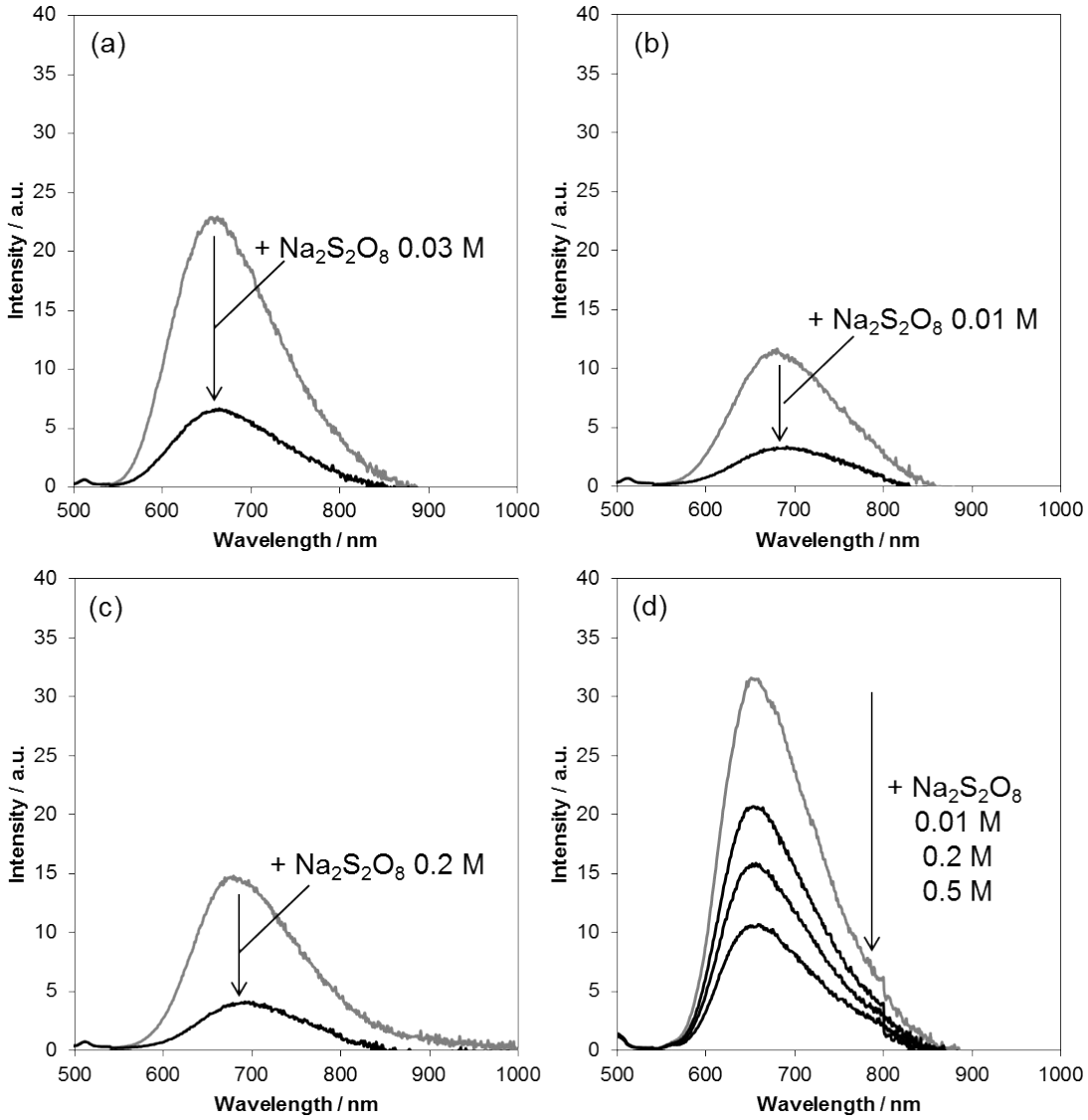

Figure S12 Phosphorescence quenching of Ru(X)-BPy-PMOs with (a) X = H, (b) X = Me, (c) X = *t*-Bu, (d) X = CO_2Me in H_2O (2 mg/ 10 mL) in the presence of $NaSO_4$ (0.049 M).

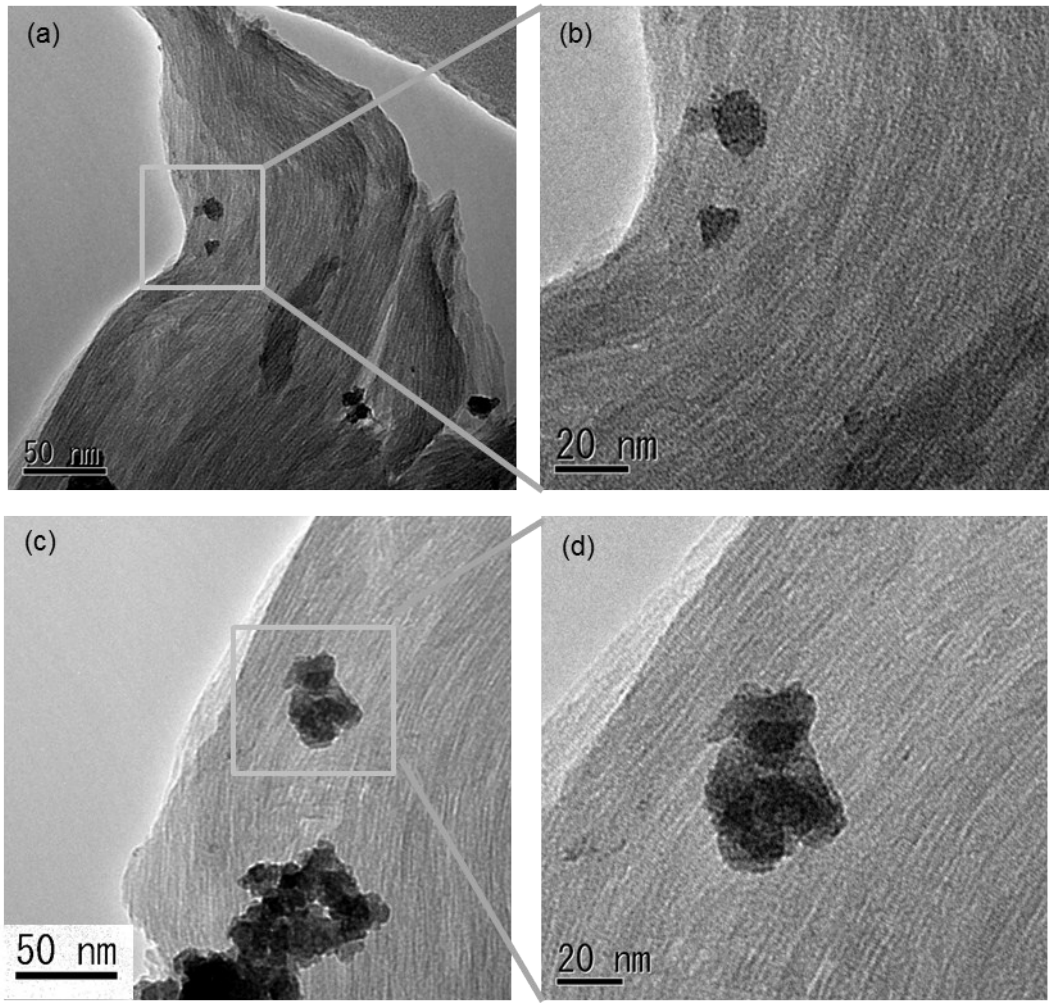

Figure S13 TEM image of Ru(CO_2Me)-BPy-PMO after photoirradiation for 24 h.

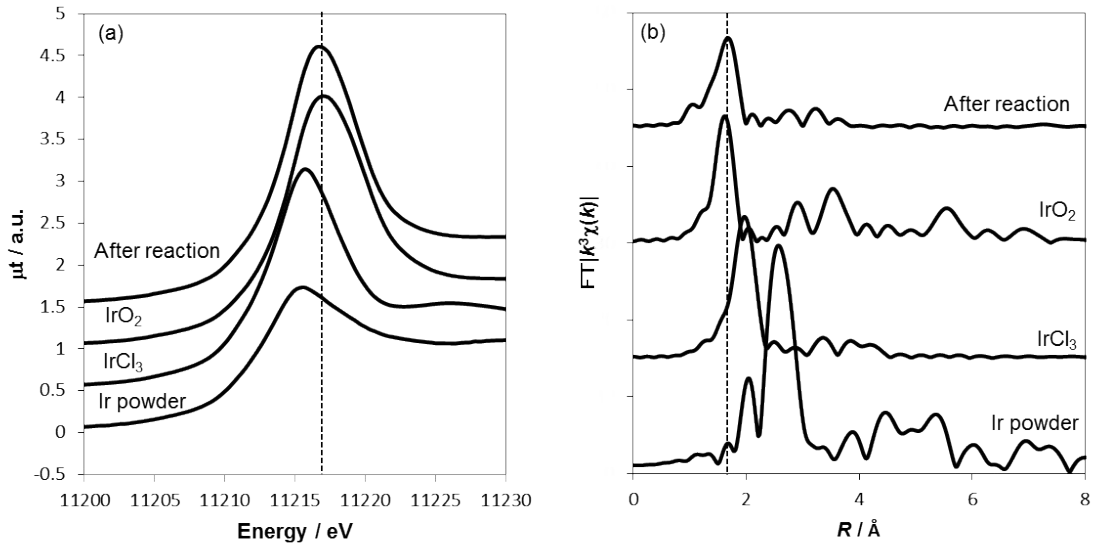

Figure S14 (a) Ir L_{III}-edge XANES spectra and (b) Fourier transforms of Ru(CO_2Me)-BPy-PMO with IrO_x after photoirradiation and control Ir species.

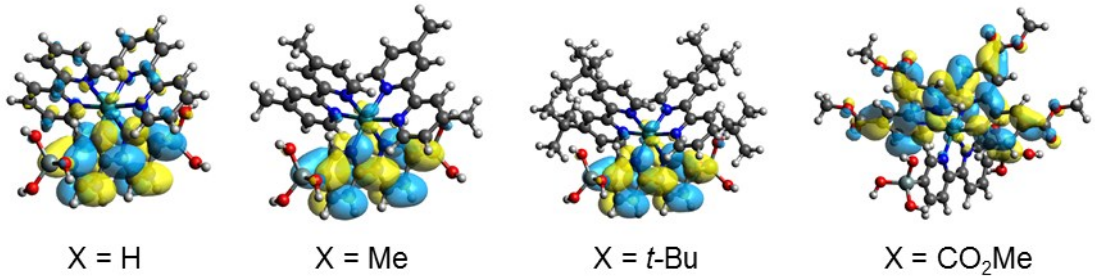

Figure S15 The highest occupied molecular orbitals in the first triplet excited states of RuBP(X) (X = H, Me, *t*-Bu and CO_2Me). The orbitals are singly occupied and represent the distributions of the excited electrons.

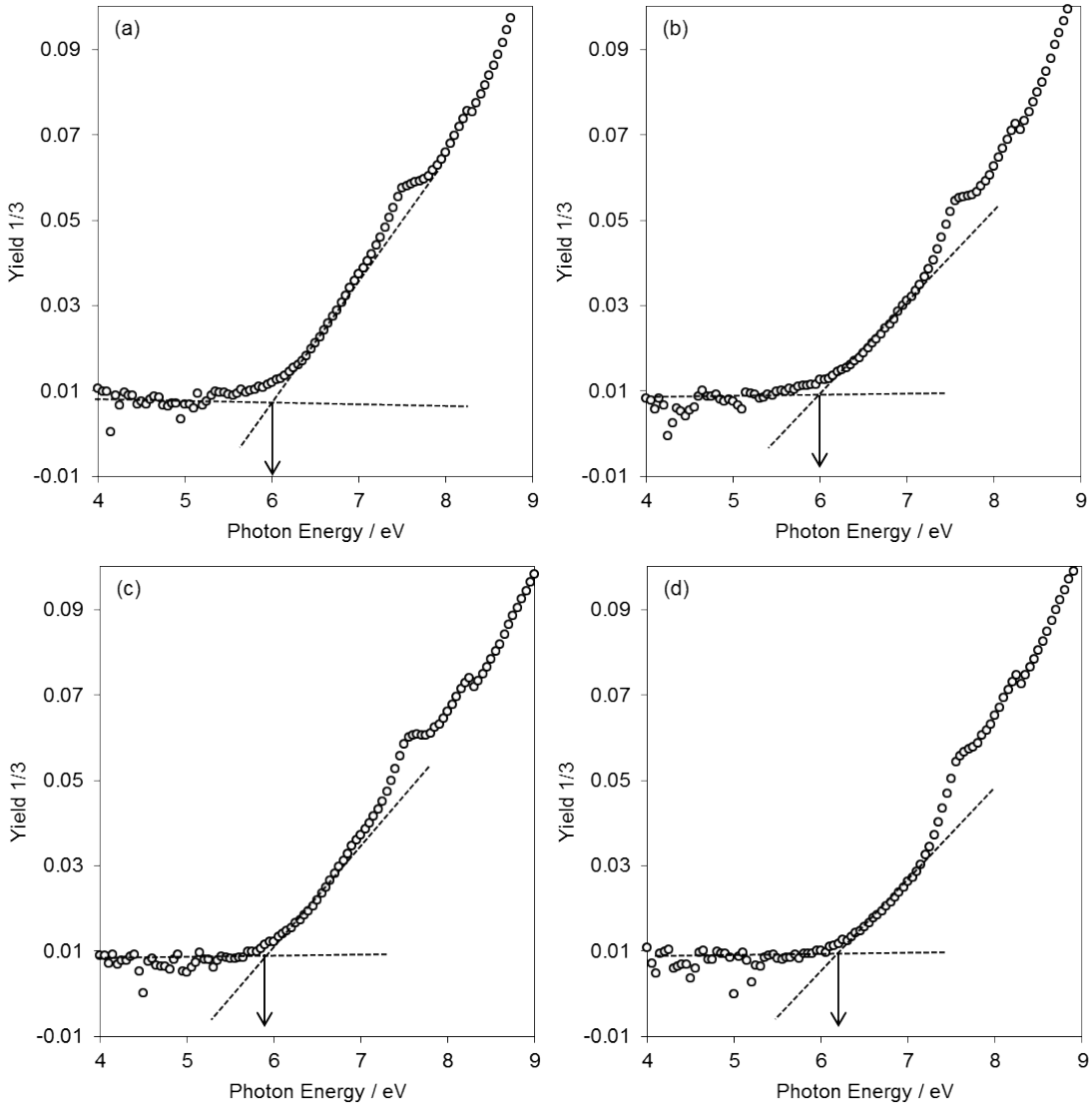

Figure S16 Ionization potential for Ru(X)-BPy-PMOs. (a) X = H, (b) X = Me, (c) X = *t*-Bu, (d) X = CO_2Me.

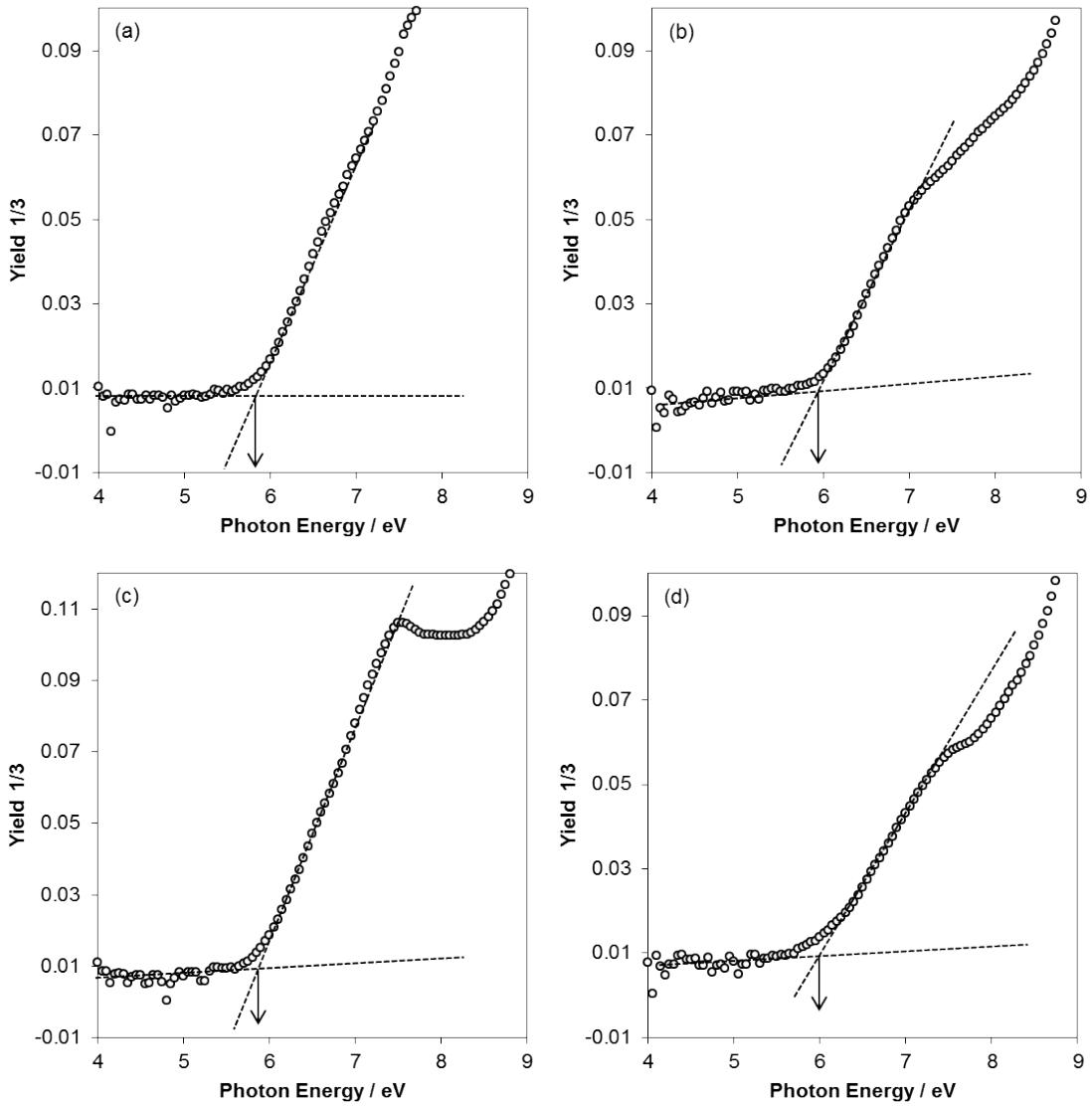

Figure S17 Ionization potential for (a) $Ru(bpy)_3Cl_2$, (b) $[Ru(dmbpy)_2(bpy)](PF_6)_2$, (c) $[Ru(dtbbpy)_2(bpy)(PF_6)_2$, (d) $Ru(dmcbpy)_2(bpy)(PF_6)_2$.

Table S2 IP values of Ru(X)-BPy-PMO and homogeneous Ru complexes.

Complex	IP
Ru(H)-BPy-PMO	6.08
Ru(Me)-BPy-PMO	5.98
Ru(*t*-Bu)-BPy-PMO	5.90
Ru(CO_2Me)-BPy-PMO	6.18
Ru(bpy)$_3$Cl$_2$	5.86
Ru(dmbpy)$_2$(bpy)(PF_6)$_2$	5.94
Ru(dtbbpy)$_2$(bpy)(PF_6)$_2$	5.87
Ru(dmcbpy)$_2$(bpy)(PF_6)$_2$	5.98

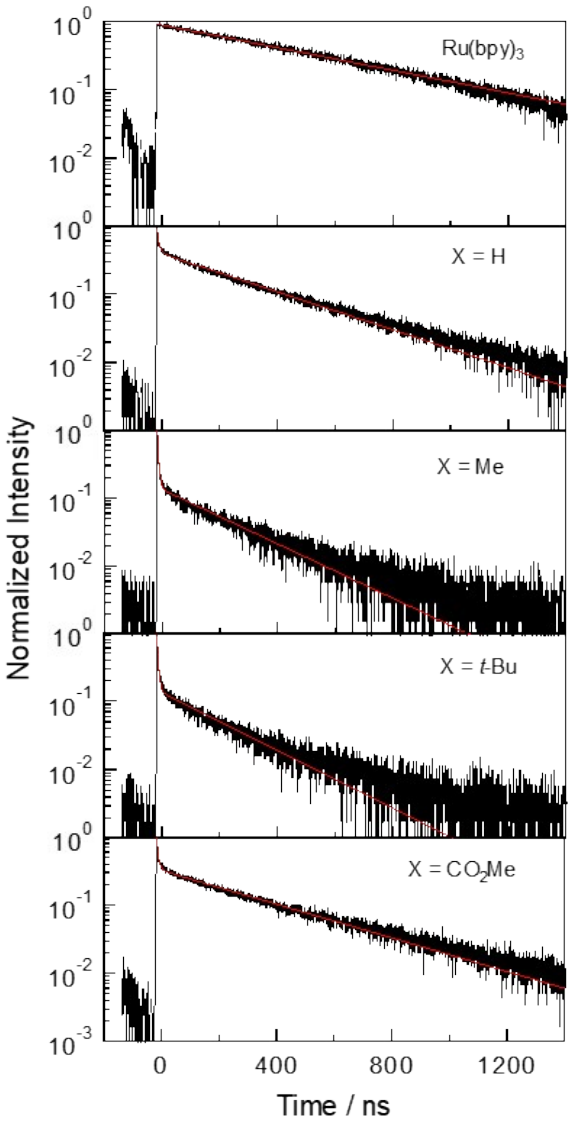

Figure S18 Phosphorescence decay profiles of Ru(X)-BPy-PMOs (X = H, Me, *t*-Bu, and CO_2Me) in H_2O at room temperature, monitored at 600 nm upon excitation at 400 nm. The decay curves were successfully analyzed by a double-exponential function. A long lifetime was assigned to the Ru complex and a short lifetime to the BPy moieties in the PMO framework.

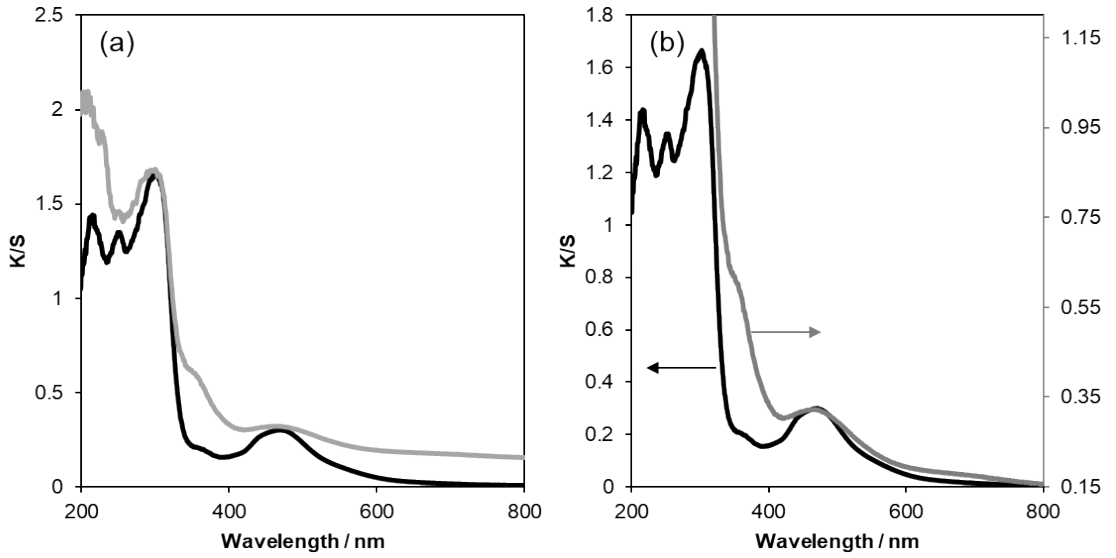

Figure S19 (a) UV/Vis diffuse reflectance spectra of Ru(CO_2Me)-BPy-PMO before and after photocatalysis reaction for 24 h, and (b) normalized MLCT bands in 400-600 nm. Black line: before reaction, gray line: after reaction.